https://doi.org/10.1016/j.ultrasmedbio.2018.07.013

● *Original Contribution*

PULSE WAVE IMAGING IN CAROTID ARTERY STENOSIS HUMAN PATIENTS *IN VIVO*

RONNY X. LI,* IASON Z. APOSTOLAKIS,* PAUL KEMPER,* MATTHEW D.J. McGARRY,* ADA IP,*
EDWARD S. CONNOLLY,[†] JAMES F. McKINSEY,[‡] and ELISA E. KONOFAGOU*,[§]

* Ultrasound and Elasticity Imaging Laboratory, Department of Biomedical Engineering, Columbia University, New York,
New York, USA; [†] Department of Neurologic Surgery, New York−Presbyterian Hospital/Columbia University Medical Center,
New York, New York, USA; [‡] Division of Vascular Surgery and Endovascular Interventions, New York−Presbyterian Hospital/
Columbia University Medical Center, New York, New York, USA; and [§] Department of Radiology, Columbia University Medical
Center, New York, New York, USA

Abstract——Carotid stenosis involves narrowing of the lumen in the carotid artery potentially leading to a stroke, which is the third leading cause of death in the United States. Several recent investigations have found that plaque structure and composition may represent a more direct biomarker of plaque rupture risk compared with the degree of stenosis. In this study, pulse wave imaging was applied in 111 (n = 11, N = 13 plaques) patients diagnosed with moderate (>50%) to severe (>80%) carotid artery stenosis to investigate the feasibility of characterizing plaque properties based on the pulse wave-induced arterial wall dynamics captured by pulse wave imaging. Five (n = 5 patients, N = 20 measurements) healthy volunteers were also imaged as a control group. Both conventional and high-frame-rate plane wave radiofrequency imaging sequences were used to generate piecewise maps of the pulse wave velocity (PWV) at a single depth along stenotic carotid segments, as well as intra-plaque PWV mapping at multiple depths. Intra-plaque cumulative displacement and strain maps were also calculated for each plaque region. The Bramwell−Hill equation was used to estimate the compliance of the plaque regions based on the PWV and diameter. Qualitatively, wave convergence, elevated PWV and decreased cumulative displacement around and/or within regions of atherosclerotic plaque were observed and may serve as biomarkers for plaque characterization. Intra-plaque mapping revealed the potential to capture wave reflections between calcified inclusions and differentiate stable (*i.e.,* calcified) from vulnerable (*i.e.,* lipid) plaque components based on the intra-plaque PWV and cumulative strain. Quantitatively, one-way analysis of variance indicated that the pulse wave-induced cumulative strain was significantly lower ($p < 0.01$) in the moderately and severely calcified plaques compared with the normal controls. As expected, compliance was also significantly lower in the severely calcified plaques regions compared with the normal controls ($p < 0.01$). The results from this pilot study indicated the potential of pulse wave imaging coupled with strain imaging to differentiate plaques of varying stiffness, location and composition. Such findings may serve as valuable information to compensate for the limitations of currently used methods for the assessment of stroke risk. (E-mail: ek2191@columbia.edu)   © 2018 World Federation for Ultrasound in Medicine & Biology. All rights reserved.

Key Words: Pulse wave imaging, Pulse wave velocity, Atherosclerosis, Calcified plaque, Arterial wall motion, Arterial wall elasticity maps, Arterial compliance, High-frame-rate ultrasound.

INTRODUCTION

Atherosclerosis is a chronic vascular disease characterized by compositional changes in the arterial walls that lead to the buildup of plaque, which consists of lipids, cholesterol, calcium and other substances found in the blood (Libby et al. 2011; Mahmoud et al. 2013). Carotid stenosis is a narrowing of the lumen in the carotid artery usually caused by atherosclerosis, occluding blood flow to the brain. A stroke may occur if the plaque ruptures and forms a blood clot (*i.e.,* cerebral thrombosis), which may detach and become lodged upstream in the smaller vessels of the brain (*i.e.,* cerebral embolism). More than 15 million people suffer strokes each year worldwide, resulting in ∼5 million deaths (Mughal et al. 2011). In the United States, stroke affects approximately 795,000 people

---

Address all correspondence to: Elisa E. Konofagou, Department of Biomedical Engineering, 351 Engineering Terrace, 1210 Amsterdam Avenue, Mail Code: 8904, New York, NY 10027, USA E-mail: ek2191@columbia.edu

each year and is the third leading cause of death ($>$140,000 annually). An estimated 15% to 20% of all ischemic strokes are attributed to carotid atherosclerosis (Taussky et al. 2011).

In patients exhibiting severe carotid blockage, a surgical intervention such as a carotid endarterectomy (CEA) or carotid stenting may be performed to reduce the risk of stroke. Current clinical practice for selecting patients for a CEA is heavily based on symptomatology and the degree of stenosis (Chan et al. 2014). However, the majority of ischemic stroke cases occur because emboli originating from a carotid plaque occlude an artery supplying the brain, not because of the luminal narrowing itself (Moller et al. 2012). Thus, a significant diameter reduction may not always correlate with a high risk of stroke. In fact, histopathological studies have found that cerebrovascular events can also occur in patients with carotid plaques causing low-grade stenosis (<30%) and with no other identifiable cause for their stroke (Lovett et al. 2004a, 2004b; Wasserman et al. 2005). As a result, nearly 80% of the ischemic strokes attributed to carotid atherosclerosis occur in asymptomatic patients without a history of stroke or transient ischemic attacks (*i.e.,* "mini-strokes") (Taussky et al. 2011). For symptomatic patients with <70% stenosis and for asymptomatic patients, the degree of stenosis alone may not be a reliable measure of stroke risk (Xu et al. 2014). Identification of patients with high-risk asymptomatic carotid plaques remains an elusive but essential step in stroke prevention.

Several recent investigations have found that the plaque structure and composition may represent a more direct biomarker for the development of cerebrovascular ischemic events rather than the degree of luminal stenosis (Naghavi et al. 2003; Saba et al. 2014). Thus, the early detection of carotid atherosclerotic disease and reliable identification of plaque features associated with an increased risk of rupture are crucial for stroke prevention. Atherosclerotic plaques can be broadly categorized into vulnerable and stable (Finn et al. 2010). Vulnerable (*i.e.,* unstable) plaques are often characterized by a thin fibrous cap covering a large necrotic core containing macrophages and interstitial collagen (van den Oord et al. 2014), leading to an increased risk of rupture. Stable plaques tend to be asymptomatic (Ross 1993) and are characterized by an intact and thick fibrous cap consisting of smooth muscle cells in an extracellular matrix rich in type I and III collagen (Finn et al. 2010). Calcification is common in late-stage atherosclerotic plaques and increases with age (Bentzon et al. 2014). The combination of calcium deposition and the collagen-rich matrix increases the stiffness of the plaque and contributes to its stability.

Non-invasive imaging methods to assess the correlation between plaque properties and risk of stroke have been developed primarily using magnetic resonance imaging (MRI), computed tomography (CT) and ultrasound techniques (Chan et al. 2014; Underhill et al. 2010; Xu et al. 2014). For example, calcified plaques are depicted as high-intensity regions on CT angiograms, while ultrasound methods include characterization of plaques based on their acoustic properties (Brewin et al. 2014) and echogenicity (Moller et al. 2012). Studies comparing plaque histology with ultrasonography have suggested that echolucent plaques tend to be higher in lipid content and echogenic plaques contain more calcified and/or fibrous tissue (Gonçalves et al. 2004).

The majority of research on imaging-based methods to assess plaque properties focuses on identifying features from a single image rather than investigating the changes in vascular dynamics associated with different types of plaque. Pulse wave imaging (PWI) is a previously developed ultrasound elasticity imaging-based technique for the spatiotemporal mapping of pulse wave-induced arterial wall motion (Apostolakis et al. 2017a; Fujikura et al. 2007; Li et al. 2013; Luo et al. 2009; Nandlall and Konofagou 2016; Vappou et al. 2010), facilitating the measurement of local pulse wave velocity (PWV). It should be noted that although PWV is known to correlate with arterial stiffness, direct indices of arterial stiffness (*i.e.,* modulus or compliance) are also affected by geometric parameters such as diameter and thickness (Holzapfel 2006; Khamdaeng et al. 2012; Westenberg et al. 2012), which can be measured from the PWI images. The modified Moens−Korteweg equation (Korteweg 1878; Moens 1878; Fung 1997) has traditionally been used to relate PWV to the incremental elastic modulus; however, assumptions such as an infinitely long, straight, isolated and cylindrical vessel with elastic, isotropic and homogenous walls, containing a homogenous, incompressible and non-viscous fluid are compromised by carotid stenosis. Also, the wave speed (*i.e.,* PWV) in the Moens−Korteweg equation represents the speed of the wave propagation with respect to the fluid, which may not be represented by the wave propagation in the wall under turbulent flow conditions. The Bramwell−Hill model (Westenberg et al. 2012) proposed a series of substitutions relevant to the observable hemodynamic measures and was used to derive the compliance of the normal controls and each plaque region:

$$\text{Compliance} = \frac{\pi (D/2)^2}{(\rho)(\text{PWV})^2} \qquad (1)$$

where D is the diameter (measured at each scan line position), and ρ is the fluid density of blood ($\sim$1060 kg/m^3).

Early PWI studies in $CaCl_2$ and AngII-induced abdominal aortic aneurysm (AAA) mouse models

(Fujikura et al. 2007; Luo et al. 2009) revealed that the uniformity of the pulse wave propagation may serve as a valuable biomarker to differentiate between normal and diseased arteries. The feasibility of PWI in the carotid artery *in vivo* has been reported in young, healthy patients (Luo et al. 2012). PWV measurements at a segment of the left common carotid artery (CCA) away from the bifurcation in eight male volunteers ranged from 4.0 to 5.2 m/s. More recently, PWI was implemented with plane wave acquisitions that are subsequently coherently combined using coherent compounding, thus improving the accuracy and reliability of the PWV measurements at high temporal and spatial resolution (Apostolakis et al. 2017a). With this technique, good reproducibility among six healthy patients was found in the estimated carotid artery PWVs over the course of $1-3$ d (first acquisition: 3.97 ± 1.21 m/s, second acquisition: 4.08 ± 1.15 m/s). Four-dimensional PWI utilizing a 2-D array transducer with plane wave acquisitions at 2000 Hz was also introduced recently and tested in phantoms and *in vivo* in healthy patients (Apostolakis et al. 2017b). Furthermore, the arterial wall displacements themselves have been used to derive the stress−strain relationship *in vivo,* illustrating the complex mechanical interaction of the different wall constituents (Khamdaeng et al. 2012).

Strain imaging, another ultrasound-based elastographic method that involves computing the spatial gradient of the displacement map to estimate strains, provides a new level of information regarding tissue elastic properties that is an active field of research in ultrasound imaging (Zaleska-Dorobisz et al. 2014). In the context of ultrasound elasticity imaging, strain represents the deformation of soft tissue in response to an external force (Ophir et al. 1999), such as the intra-luminal pressure of a pulsating artery acting on the walls in the radial direction. When this force deforms a medium such as a heterogeneous plaque, stiffer (softer) regions in the medium are expected to experience a lower (higher) level of strain. One- and two-dimensional ultrasound strain imaging has been attempted in carotid plaques (Hansen et al. 2016; Naim et al. 2013; Poree et al. 2015; Roy Cardinal et al. 2017), illustrating both the feasibility and limitations of using peak systolic cumulative strains for plaque characterization. One of the key considerations for robust arterial wall strain estimation is the size of the strain kernel, which must be small enough to operate within the structure of interest but large enough to ensure an adequate strain signal-to-noise ratio (Bunting et al. 2014). This is why strain estimation in a thin structure such as the normal carotid artery wall typically can yield noisy estimates. However, the increased thickness in atherosclerotic regions allows for the use of larger strain kernels to achieve higher signal-to-noise ratios.

Strain estimation using ultrasound has exhibited great promise for clinical integration because of its non-invasiveness, low cost and ease of use. Two-dimensional (*i.e.,* both axial and lateral) strain estimation techniques have been developed by our group for cardiac imaging applications such as myocardial elastography (Konofagou et al. 2002; Lee et al. 2007; Lee and Konofagou 2008) and mapping of the electromechanical wave (Provost et al. 2011).

Thus, combining the results of PWI and strain imaging may lead to new insights into how arterial function is affected by plaques of various composition, size and location. The PWV in a stenotic carotid segment as well as the pulse wave-induced displacements and strains, may be useful in detecting and characterizing plaque regions. In the work described here, the PWI and strain imaging methods were applied in patients with carotid atherosclerosis to investigate the effects of stenosis on local arterial mechanics.

METHODS

Data acquisition

All imaging procedures were approved by the institutional review board of Columbia University Medical Center. Eleven patients (N = 13 plaques; 9 males, 2 females; mean age: 76.00 ± 8.51 y), diagnosed with moderate ($>50\%$ occlusion) to high-grade ($>80\%$ occlusion) carotid stenosis by a clinical expert, provided informed consent to participate in the present study. Radiofrequency signals were acquired using conventional ultrasound (SonixTouch, Analogic Corp., Peabody, MA, USA) and/or plane wave ultrasound (Vantage 256, Verasonics Inc., Kirkland, WA, USA) at a carotid segment exhibiting a clear atherosclerotic lesion on the B-mode image. In all patients, imaging was performed at either the carotid bifurcation or the common carotid artery (CCA) segment immediately below the bifurcation. For the conventional sequence, 32 scan lines were used at imaging depths of $30-50$ mm, resulting in frame rates of $423-505$ Hz. For the plane wave sequence, three or five compounding angles were used at the same imaging depth, resulting in frame rates of $1600-2700$ Hz, a range that has previously been reported to be optimal (Apostolakis et al. 2017a). A CUDA-based delay-and-sum reconstruction algorithm (Apostolakis et al. 2017a) was used to reconstruct 128 scan lines.

Five of the patients exhibiting high-grade stenosis were scheduled to undergo a CEA, which presented a unique opportunity to correlate PWI findings with the disease state. In these patients, imaging was performed 1 h to 1 wk before the scheduled operation. After surgery, the resected atherosclerotic tissue from the imaging location (either the common carotid or the bifurcation)

was collected for gross examination and hematoxylin and eosin staining using a standard protocol. The resected specimen was successfully retrieved from 4 of CEA patients.

The right and left carotids of n = 5 healthy patients (N = 20 measurements, 4 males, 1 female, mean age: 29.8 ± 7.05 y), both at the bifurcation and below the bifurcation, were imaged as a control group. Imaging was performed at the CCA segment immediately before the carotid bifurcation to be consistent with the scanning location in the stenosis patients.

Data processing

For illustrative purposes, Figure 1 depicts the results of applying the methodology used throughout the present study to a healthy carotid artery close to the bifurcation. Axial displacements were estimated offline with a 1-D cross correlation-based motion estimation method (Luo and Konofagou 2010). Axial wall displacements overlaid onto the corresponding B-modes are provided in Figure 1a−c. Subsequently, the anterior wall of the imaged vessel was manually traced, and the wall displacement waveforms at each lateral position of each arterial wall trace were sequentially stacked, generating a 2-D spatiotemporal plot that depicts the displacement variation over distance and time of the pulse wave propagation. This procedure was repeated for the posterior wall, and the two resulting spatiotemporal plots were subtracted, generating a distension spatiotemporal plot and eliminating any rigid motion of the vessel (Fig. 1e). The slope of the linear regression of the relationship between the 50% upstroke arrival time point and the length of the imaged carotid segment yielded the slope as the regional PWV (Fig. 1e).

The presence of plaques, however, may induce wave reflections and flow disturbances within the
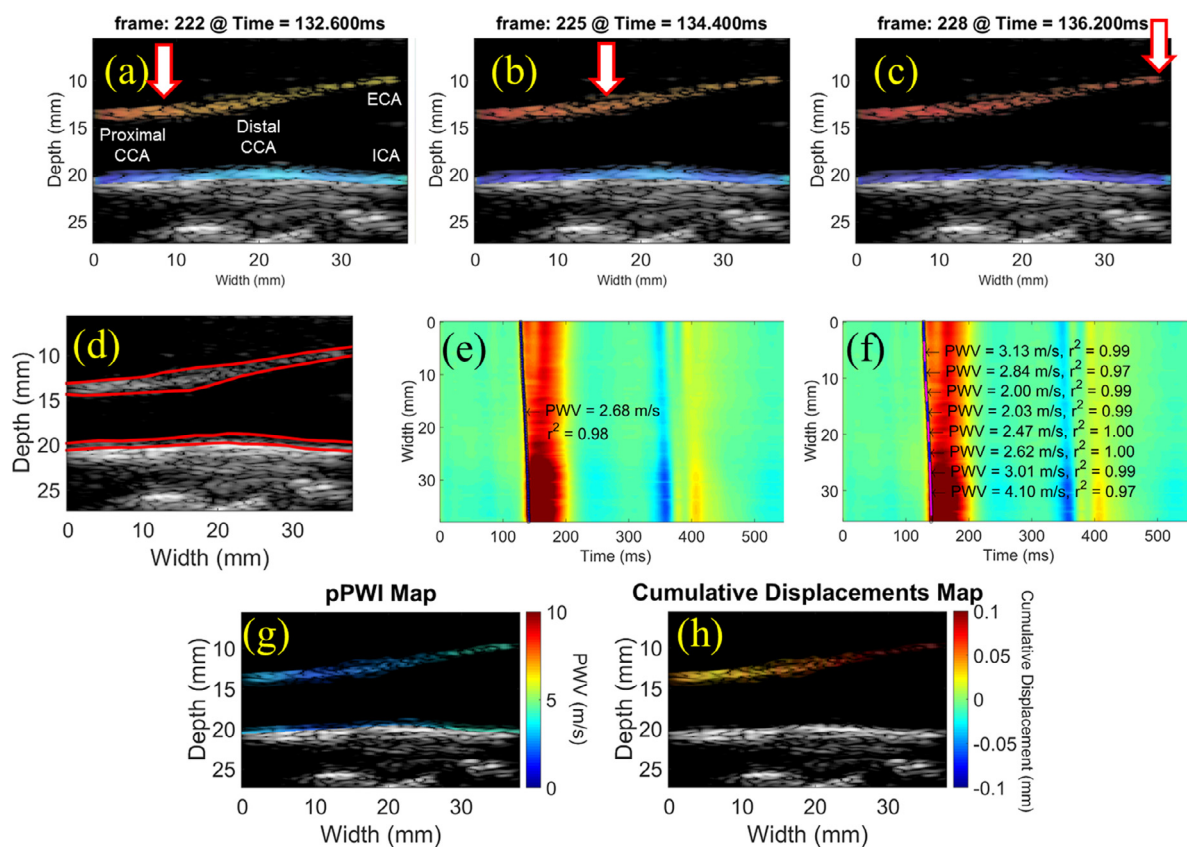
Fig. 1. (a−c) Consecutive PWI frames showing pulse wave propagation along the anterior wall of a normal carotid artery close to the bifurcation (M, 29 y old). (d) Manual segmentation and automated tracking of the inner and outer layers of the walls allow for measurement of the anterior wall thickness and inner diameter at each scan line position over time. Regional PWV estimation (e) generates a single PWV estimate across the imaged segment, while a piecewise kernel outputs an array of PWV measurements that can be color-coded and overlaid onto the B-mode (g). The maximum cumulative displacement at each pixel in the anterior wall (h) is computed by summing the inter-frame displacements from the beginning of the waveform upstroke (*i.e.,* end diastole) to the point of maximum distension (*i.e.,* peak systole). CCA = common carotid artery; ECA = external carotid artery; ICA = internal carotid artery; PWI = Pulse Wave Imaging; PWV = pulse wave velocity.

imaged carotid segment, changing the regional wave propagation behavior (Grotberg and Jensen 2004). To investigate these changes, an increased resolution of the PWV estimation was achieved using piecewise PWI (Apostolakis et al. 2016), which entailed sliding a fixed-length overlapping kernel along the spatiotemporal map and performing linear regression on only the waveform arrival times within the kernel, thus generating an array of PWV estimates along the imaged segment (Fig. 1f). The piecewise PWV measurements were then color-coded and overlaid onto the reference B-mode frame for visualization of the PWV at different points along the artery (Fig. 1g). In atherosclerotic carotid arteries with altered wall dynamics, piecewise PWV mapping may reveal drastic variations in the arterial properties based on the wave propagation around and possibly through the plaque.

The maximum cumulative displacements were then computed within user-defined regions of interest (ROIs) on the ultrasound image, such as a plaque or a segment of the normal carotid wall (Fig. 1h). The same 1-D cross-correlation method used for automated wall tracking based on the inter-frame displacements was applied to track each pixel of the ROI in the axial direction across the entire sequence of images. By integrating the inter-frame displacements to obtain the cumulative displacements within the ROI at peak systole, the stiffness contrast may be detected along the imaged segment. Stiff, calcified plaques were expected to displace less than normal carotid arteries as well as softer, lipid-rich plaques.

The 1-D axial strain within a ROI was obtained using a least-squares strain estimator (Kallel and Ophir 1997) to compute the spatial gradient of the 1-D cumulative displacements. Negative strains indicated radial tissue compression, whereas positive strains indicate radial tissue elongation. Simultaneous negative and positive strains denote plaque bulking.

Intra-plaque strains were computed using a strain kernel that was half the mean thickness of the plaque region. The cumulative strain corresponding to maximum cumulative displacement was obtained for each pixel in the plaque ROI. In this way, intra-plaque properties may also be investigated by estimating the deformation of plaque components induced by the arterial pulsation. This may potentially reveal information about intra-plaque properties such as calcified inclusions and/or lipid pools based on the hypothesis that the spatiotemporal map from different depths may be altered by the heterogeneity of certain plaque regions. Intra-plaque PWV maps were generated by manually segmenting the inner and outer layers of the arterial walls in the first frame of the imaging sequence as in Figure 1d, thus accounting for the reduced diameter and increased thickness in plaque regions along the artery. Multiple wall traces (and, hence, spatiotemporal maps) were automatically generated between the layers, and the piecewise PWV measurements obtained from each spatiotemporal map were overlaid onto the B-mode reference frame, forming an image of the PWV at different depths within the plaque region(s).

Subsequently, regional compliance values were estimated using the Bramwell−Hill equation (1). It should be noted that because diameter is changing throughout the cardiac cycle (Polak et al. 2012), all compliance calculations in this study were performed using the maximum diameter. This corresponds to the peak systole phase of the cardiac cycle and represents the maximally distended artery, which is physiologically relevant for cardiovascular function analysis (Cunha et al. 1995; Segers et al. 2004). As mentioned in the Introduction, the echogenicity and acoustic shadowing on the B-mode image served as a crude criterion for identifying different types of plaques. More specifically, calcified plaques gave the most intensive echoes and attenuated the ultrasound signal distal to the plaque, causing significant acoustic shadowing (Strandness 1994). Lipid-laden plaques were frequently represented as echolucent lesions and often presented an echogenic border at the lumen−intima interface corresponding to the fibrous cap (Fioranelli and Frajese 2012). In each of the atherosclerotic carotid arteries imaged, the degree of calcification in the plaque region was graded based on visual assessment of the echogenicity and the severity of acoustic shadowing on the B-mode image. Additionally, given that no exact value for degree of stenosis was provided (*i.e.,* only >50% or >80%) and also to ensure that the measurement corresponds to the plaque within the field of view, the degree of stenosis value was re-estimated by performing diameter measurements on the B-mode at the maximum stenotic part and at a nearby non-stenotic section.

Finally, in patients for whom prior CTA scans were available, the image intensity of the plaque region(s) was also visually assessed for confirmation of the degree of calcification, because calcified plaques show up as regions of very high brightness on the CTA. However, beam-hardening and blooming artifacts have made it difficult to accurately assess the degree of luminal narrowing by CTA in the presence of heavily calcified plaques (Zhang et al. 2008).

Statistical analysis

One-way analysis of variance with the Bonferroni multiple comparison test was used to determine statistical significance between the cumulative displacement, strain and compliance measurements in the non-calcified, moderately calcified and severely calcified plaque cases and the normal controls.

RESULTS

Figures 2 and 3 illustrate the displacement and single-depth PWV mapping results in two patients (72-y-old female and 76-y-old male, respectively), obtained using the conventional imaging sequence. In both cases, decreased cumulative displacements (Figs. 2b and 3b) were observed in the plaque of interest (*red contour*). Also in both cases, the piecewise PWV map (Figs. 2c, d and 3c, d) reveals a region where the PWV transitions from positive (*i.e.,* proximal to distal) to negative (*i.e.,* distal to proximal) as if two waves traveling in opposite directions are converging (*white arrow*). In Figure 2, this point of convergence occurs within the plaque, whereas in Figure 3, the convergence point occurs immediately before the plaque. This is an interesting phenomenon that was also observed in other cases and may serve as a biomarker for plaque characterization.

The intra-plaque displacement, strain and PWV mapping results for three CEA cases—one moderately calcified plaque (56-y-old male) in Figure 4, one severely calcified plaque (80-y-old male) in Figure 5 and one lipid plaque (75-y-old male) are illustrated in Figure 6. The CTA for the moderately calcified case (Fig. 4a) revealed the presence of two calcified inclusions within the plaque

ROI. For the severely calcified and lipid cases, the resected specimen was obtained after CEA (Figs. 5c and 6c, respectively) to confirm the presence of a heavily calcified region (*blue box* in Fig. 5c) and fatty necrotic core (*blue box* in Fig. 6c). In both calcified cases, a region of alternating positive and negative PWVs was observed along the depth direction of the plaque (*white arrows* in Figs. 4f and 5f), while the intra-plaque PWV map for the lipid case revealed relatively uniform PWVs along the depth direction. Also, in the lipid case, the intra-plaque strain map was able to differentiate the fibrous cap (*white arrow* in Fig. 6b, e) from the necrotic core (*red arrow* in Fig. 6b, e) based on compression of the fibrous cap (*i.e.,* blue strain) and radial elongation of the fluid-like fatty core (*i.e.,* red/yellow strain).

Quantitative results

Figure 7 illustrates the pulse wave-induced displacement (a) and strain (b) for all 13 plaque regions found in the 11 stenosis patients, compared with the 20 normal carotid artery acquisitions in the control group. The pulse wave-induced cumulative displacement was significantly higher in the moderately calcified plaques than in the non-calcified and severely calcified plaques,
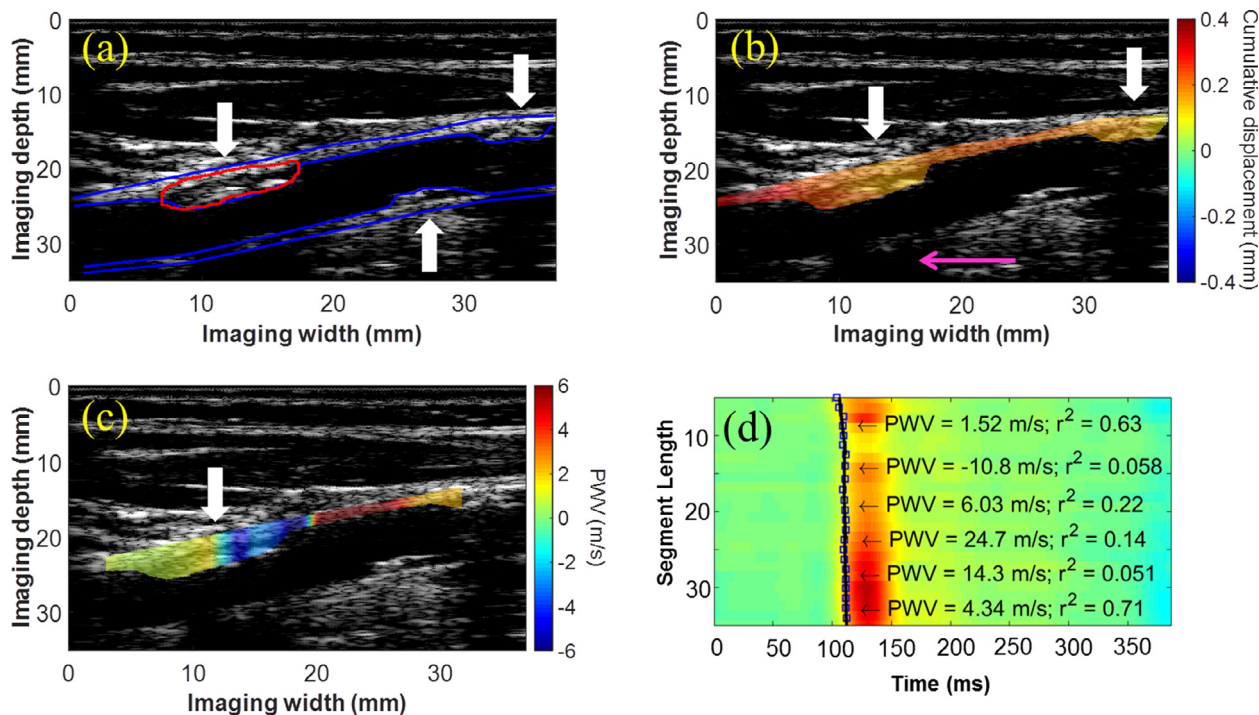

Fig. 2. (a) B-Mode from the right common carotid artery of a 72-y-old woman (50%−79% stenosis) containing atherosclerotic lesions on both the anterior and posterior walls (*white arrows*). (b) Decreased cumulative displacement was observed in the anterior wall plaques (*white arrows*). The presence of the acoustic shadow (*pink arrow*) obstructing a portion of the posterior wall suggests that the plaque directly above is moderately calcified. (c) The PWV map reveals a region where the wave appears to converge inside the plaque (*white arrow*). (d) Piecewise PWV measurements overlaid on the spatiotemporal map. PWV = pulse wave velocity.
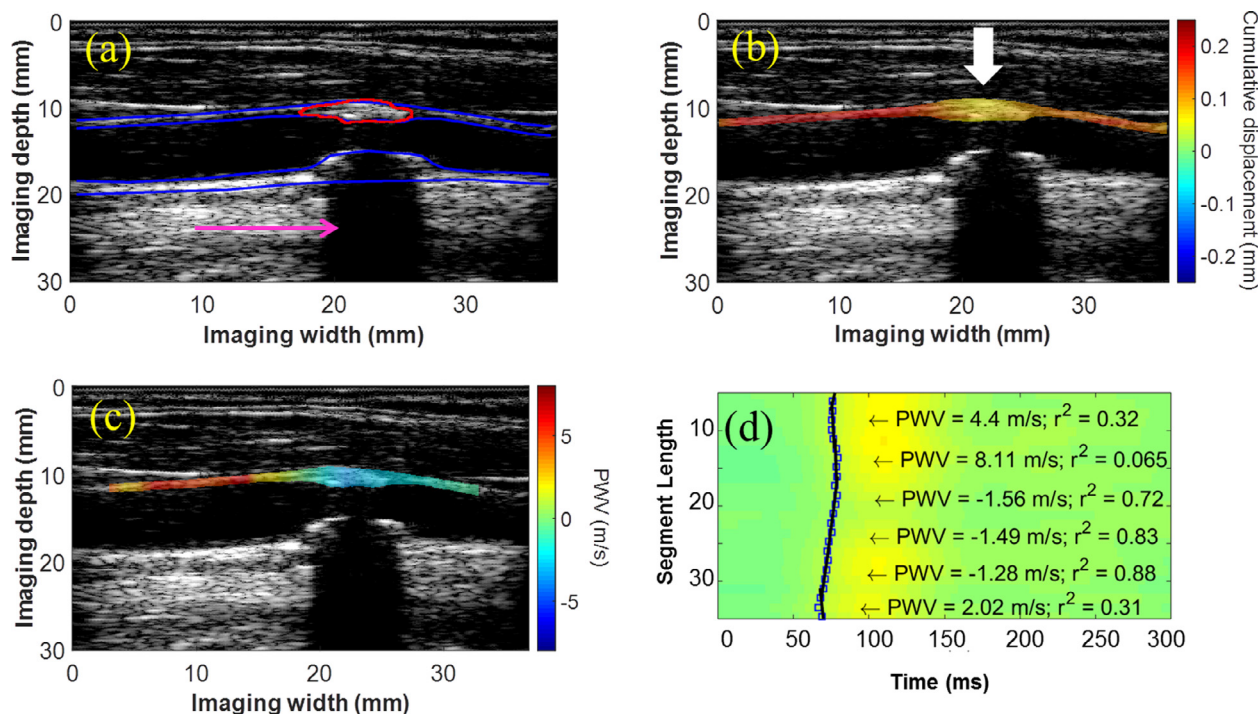
Fig. 3. (a) B-Mode image, (b) displacement map and (c) PWV map from the right common carotid artery of a 76-y-old man obtained using a conventional ultrasound sequence. The *pink arrow* points to the acoustic shadow caused by the calcified posterior wall plaque, and the *white arrow* indicates a region of decreased displacement or pulse wave convergence. (d) Piecewise PWV measurements overlaid on the spatiotemporal map. PWV = pulse wave velocity.

whereas cumulative strain was significantly lower ($p < 0.01$) in the moderately and severely calcified plaques compared with the normal controls. Figure 7c illustrates that the degree of stenosis varied between non-calcified, moderately calcified and severely calcified plaques, with the mean values being 71%, 33% and 60%, respectively.

Figure 8 illustrates that, as expected, compliance was significantly lower in severely calcified plaque regions compared with the normal controls ($p < 0.01$)

DISCUSSION

Non-invasive methods that can reveal new information regarding the composition and stability of carotid plaques may play a key role in plaque characterization and stroke prevention. In this study, the feasibility of PWI was evaluated in patients with moderate to severe carotid stenosis. To increase the resolution of the wave propagation analysis for the detection and characterization of regional lesions, piecewise estimation of the PWV was used. The high spatial and temporal resolution achievable using plane wave architecture led to the development of intra-plaque PWV mapping, where multiple wall traces through the plaque were generated to investigate if and how the spatiotemporal maps at different depths were affected by inhomogeneities within the plaque.

One of the observations from the single-depth PWV maps (Figs. 2 and 3) was that the PWV may appear higher around the plaque rather than within the plaque itself. For example, Figure 2c reveals regions of high PWV in the normal wall segment after the plaque, whereas Figure 3c reveals regions of high PWV in the normal segment preceding the plaque. This may be explained by several physiologic and imaging-related factors that must be taken into consideration when interpreting the measurements provided by PWI, such as the turbulent flow arising from local geometric and mechanical changes of the artery in the presence of plaque (Tan et al. 2008).

In fluid mechanics, turbulence is characterized by a high Reynold's number (*i.e.,* >4000), which is a dimensionless quantity that is used for the prediction of flow patterns in various situations (Fung 1997). Although much of the hemodynamics in a healthy human body exhibits laminar flow (*i.e.,* Reynolds number <2100), turbulent flow is observed at some specific locations (such as the carotid bifurcation) and in the presence of atherosclerotic disease (Hutchinson and Karpinsky 1985). Simulations of stenosed carotid bifurcations using pulsatile inlet conditions have revealed the presence of vortices and oscillatory flow reversal distal to the region of stenosis (Lee et al. 2008). Because blood is
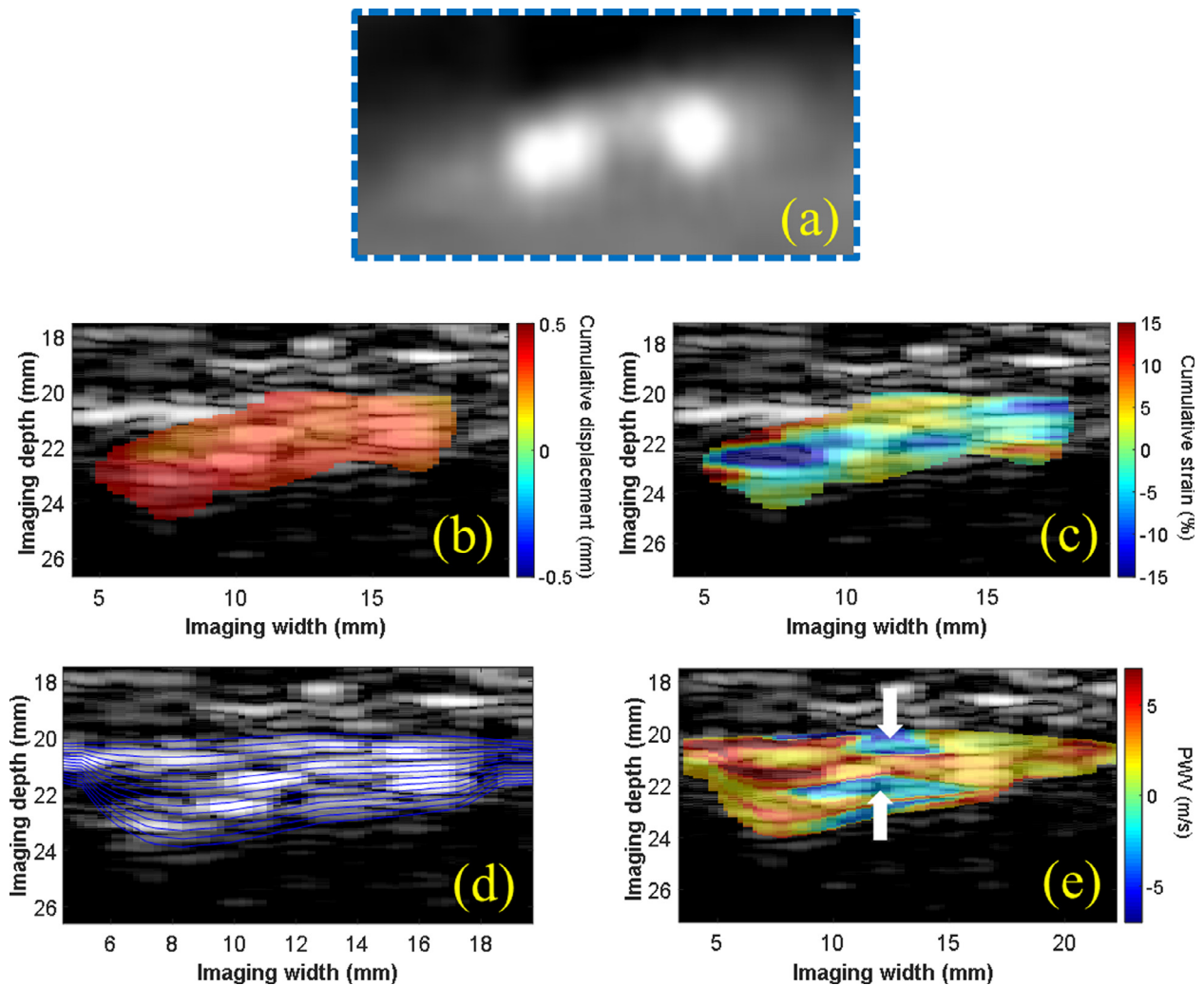
Fig. 4. (a) Computed tomography angiography image of a plaque region in the right common carotid artery in a 56-y-old man taken 2 wk before ultrasound imaging. The intra-plaque cumulative displacements (b) appeared uniformly distributed within the plaque region of interest, while regions of tissue compression (*blue*) and elongation (*red*) were observed on the cumulative strain map. (d) Multiple wall traces were generated for intra-plaque PWV mapping. The PWV map (e) reveals regions of negative PWV (*white arrows*) between regions of positive PWV that appear to correlate with the two calcified inclusions observed on the enlarged computed tomography angiography image (a). PWV = pulse wave velocity.

incompressible, blood flow in the arterial lumen must accompany regional wall motion during the cardiac cycle (Luo and Konofagou 2011). Thus, although wave propagation along the wall of a normal carotid artery is driven by laminar flow, the effects of turbulent flow in a stenotic artery may be manifested in its wall motion, particularly around stiff plaques exhibiting very little pulse wave-induced displacement.

In addition to causing turbulent flow conditions, the carotid bifurcation, cerebral vascular system, regions of stenosis and other arterial stiffness inhomogeneities also serve as significant sources of wave reflection (Bleasdale et al. 2003; Ino-Oka et al. 2009). Especially given the increased spatial variation of the arterial mechanical properties in atherosclerotic carotids, wave reflections are expected to be more prevalent (Meinders et al. 2001). The pulse waveform at any given site in the arterial tree is a combination of the forward wave and any reflected waves originating from further down the vasculature (Nichols et al. 2011). These waves are propagating at speeds on the order of meters/second within a roughly 38-mm-long segment of the stenotic carotid artery (*i.e.*, equal to the width of the linear array transducer), generating multiple waves that may reflect and merge over the course of the cardiac cycle, particularly in a case like that illustrated in Figure 2, where more than one plaque region was identified on the anterior wall. Thus, the composite pulse waveform at different scan line
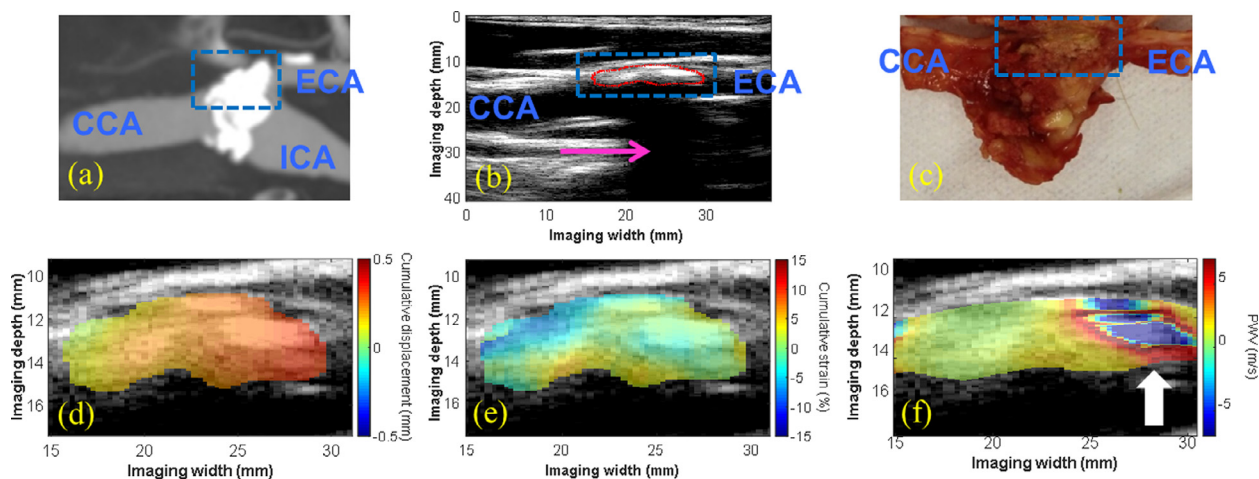
Fig. 5. (a) Computed tomography angiography image revealing a severely calcified, high-grade stenosis (80%−99%) at the carotid bifurcation in an 80-y-old man generating a severe acoustic shadow (*pink arrow* in b). A highly calcified white nodule was identified on the gross pathology image (*blue dashed box* in c), correlating with the echo-reflective region of the plaque on the B-mode (*red contour* in b). The intra-plaque displacement (d) and strain (e) maps revealed regions of varying displacement and strain amplitude, whereas the intra-plaque PWV map revealed a region of alternating positive and negative PWVs throughout the depth of the plaque at the distal end (*white arrow* in f). PWV = pulse wave velocity.

positions along a stenotic carotid artery may be influenced by different turbulent, reflective and dispersive conditions, resulting in different wave speeds measured by PWI. Moreover, complex arterial motion around stenotic segments has been previously reported in a phantom study by Binns and Ku (1989) where simultaneous expansion and collapse of the stenotic vessel have been reported before and after the stenotic segment, respectively. Figure 4c illustrates the appearance of both positive and negative PWVs between two calcified inclusions, indicating that such complex phenomena may be able to be captured using intra-plaque PWI.

Turbulence, flow reversal and reflected waves around the plaque may have also given rise to the
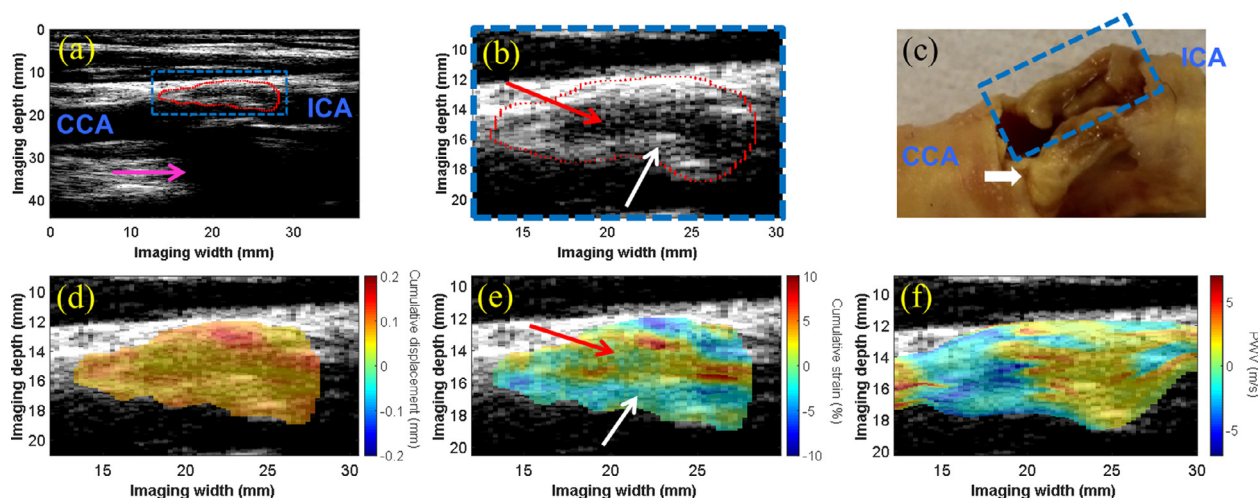

Fig. 6. (a) B-Mode image of the carotid bifurcation in a 75-y-old man reveals the plaque (*red contour*) situated at the bifurcation and extending into the proximal internal carotid artery. Acoustic shadowing (*pink arrow*) is observed. (b) An enlarged image of the plaque region of interest (*blue box* in a) reveals an echolucent region (*red arrow*) surrounded by an echogenic border indicative of the fibrous cap (*white arrow*). (c) Gross pathology reveals bilateral plaques with liquid-like fatty substance oozing from the plaque of interest (*blue dashed box*). The white calcified nodule (*yellow*) in the far wall plaque is likely the main contributor to the acoustic shadowing observed in (a). The intra-plaque cumulative displacement map (d) is mostly uniform, while the cumulative strain map (e) reveals compression in the solid fibrous cap (*white arrow*) and elongation in the liquid-like fatty region (*red arrow*). The intra-plaque PWV map (f) revealed a transition from negative PWV to positive PWV in the direction of wave propagation at all depths of the plaque.
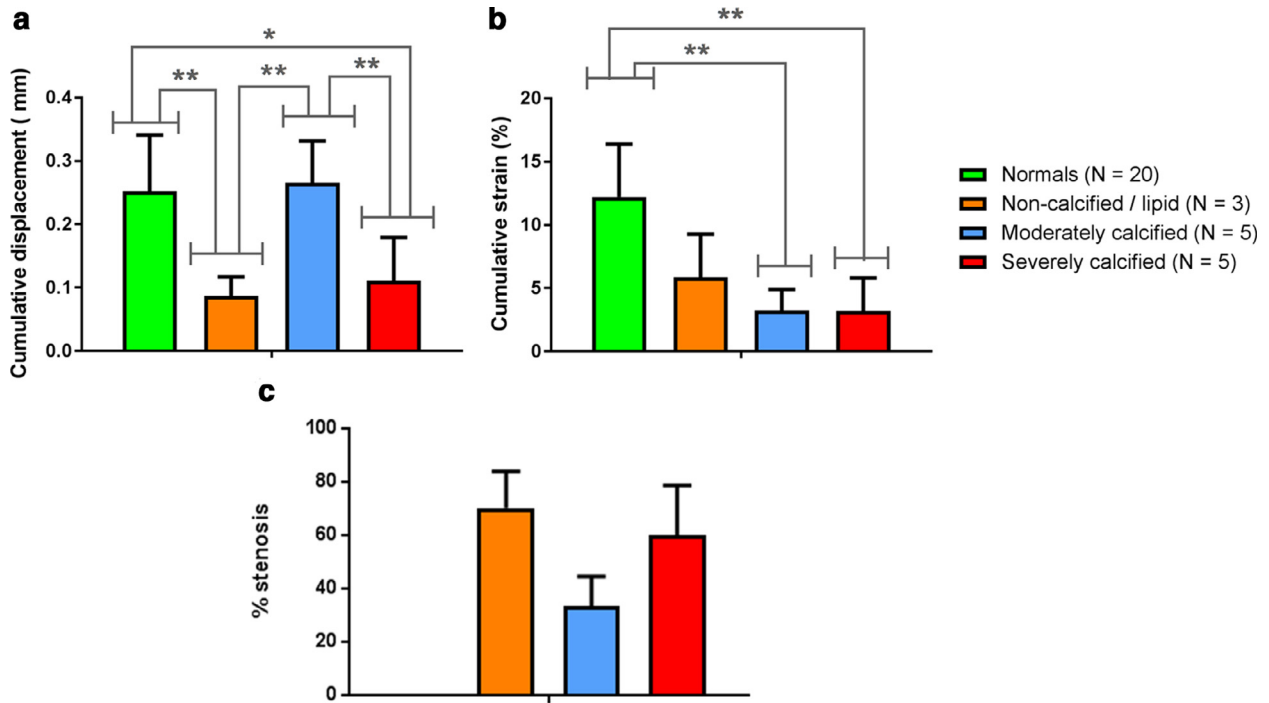
Fig. 7. (a) Cumulative displacement and (b) cumulative strain were computed within the normal carotid wall for the control group and within the 13 plaque regions for each of the stenosis patients. *Statistically significant at $p < 0.05$. **Statistically significant at $p < 0.01$, computed using Bonferroni's multiple comparison test. (c) Degree of stenosis measured from the B-mode image.

negative PWVs that were observed in Figures 2c and 3c. In these cases, the positive and negative PWVs converged at different points (within the plaque in Fig. 2c and before the plaque in Fig. 3c), indicating that locations of wave convergence may provide clues regarding plaque properties. Additionally, given that the presence of negative slopes and fluctuating 50% upstroke markers is a multifactorial phenomenon, negative PWVs cannot be singularly attributed to wave reflections and are the result of tracking the composite waveform of the pulse wave produced by the combination of the aforementioned arterial wall and blood flow dynamics.
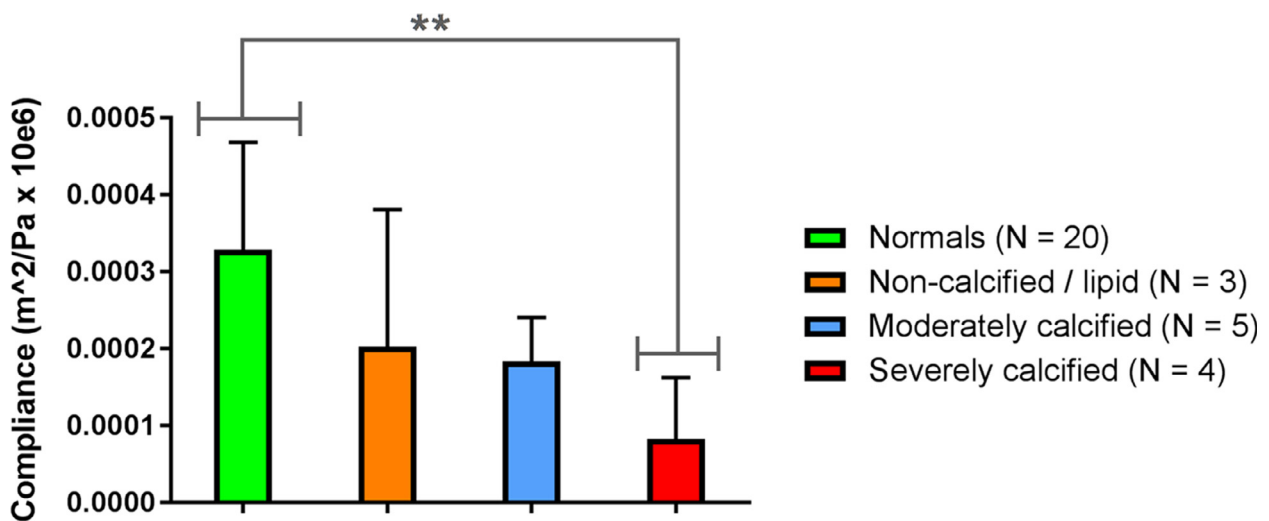

Fig. 8. Compliance was computed based on the Bramwell−Hill model at the central scan line position of the normal carotid segment for the control group and at 12 of the plaque regions for the stenosis patients. *Statistically significant at $p < 0.05$. **Statistically significant at $p < 0.01$, computed using Bonferroni's multiple comparison test.

Because blood flow imaging was not performed in this study, the fluid−solid interaction (FSI) between the blood and the wall could not be studied. The FSI is a crucial step in biomechanical modeling that couples computational fluid dynamics with finite-element analysis in tissues (Watanabe et al. 2011; Shahmirzadi and Konofagou 2012). The mechanics of the fluid and structure systems are usually coupled at the interface by the kinematic and dynamic conditions, which define the velocity, pressure and/or other parameters of the fluid and structural nodes at the interface to be the same. The increased PWV around the plaque seen in Figures 2 and 3 is an observation that warrants further investigation through comparison with FSI simulations and phantom experiments. Most FSI studies of carotid arteries and stenosis have focused on wall shear stress, wall displacement, pressure and flow velocity around the region of stenosis rather than wave propagation (Park et al. 2013; Tang et al. 2003; Teng et al. 2010).

The disturbance in wall motion induced by turbulent flow and reflection within and around the stenotic region also presents the problem of varying waveform morphology. The fact that the composite pulse waveform at different scan line positions along a stenotic carotid artery may be influenced by turbulence, reflection and dispersion means that the morphology of the waveform is changing as it propagates across a stenotic region. In previous studies (Apostolakis et al. 2017a; Li et al. 2015), PWI measurements have been validated in phantoms and *in vivo* by tracking the 50% upstroke of each waveform in the spatiotemporal map. This may work well under normal geometric conditions because wave reflections typically affect the back end (*i.e.,* downstroke) and the peak of the forward wave (Nichols et al. 2008). However, the effects of complex wave interactions under stenotic conditions on PWV estimation using PWI requires further investigation. The 50% upstroke of the waveform in the normal wall may not represent the same point as the 50% upstroke of the composite waveform near or within a plaque region in the same field of view. Thus, the choice of tracking feature may affect the PWV estimation in stenotic conditions. Ongoing work involves addressing this issue by estimating PWV with inverse problem solution-based methods (McGarry et al. 2016, 2017). Additionally, incorporating flow velocity Doppler measurements into our method will improve understanding of the complex pulse wave propagation and provide more robust arterial stiffness measurements.

Imaging location

The most common location for carotid plaque buildup is the bifurcation (Imparato 1986), which also serves as a significant reflection site for the arterial pulse wave. In cases where imaging was performed at the bifurcation, the wave propagation and induced displacements were the result of combined flow patterns caused by both the bifurcation and the plaque. This problem is further complicated by the observation that carotid bifurcation anatomy also exhibits major variation among individuals (Schulz and Rothwell 2001). Computer simulation of local blood flow and vessel mechanics in a compliant carotid artery bifurcation model revealed strong secondary wall motion in the carotid sinus (*i.e.,* the dilated area at the base of the internal carotid artery just superior to the bifurcation) (Perktold and Rappitsch 1995). This may explain why the moderately calcified cases did not exhibit significantly lower displacement than the non-calcified cases and normal controls (Fig. 7a). Furthermore, the degree of stenosis differed between non-calcified, moderately calcified and severely calcified is illustrated in Figure 7c. This difference could have also contributed to higher displacement values in the moderately calcified plaques with lower degree of stenosis. More specifically, this indicates that there is less overall material embedded in the diseased arterial wall, thus limiting the impact of atherosclerosis on arterial distensibility. Consequently, this may be the reason behind the observation that arterial wall motion was not significantly affected. However, as expected, the plaque regions exhibited significantly lower strain (Fig. 7b) and compliance (Fig. 8) than the normal controls.

When all the above factors are taken into account, the complexity of the arterial mechanics and dynamics in the presence of plaques becomes apparent. The effective characterization of plaques will likely rely on a combination of different imaging methods. In the presence of heavily calcified plaques, blooming artifacts on the CTA (Oliver et al. 1999) and acoustic shadowing on the B-mode ultrasound image hinder the ability of both modalities to visualize the plaque. The high-intensity brightness on the CTA exaggerates the degree of stenosis, while the attenuation of the ultrasound signal by a calcification limits the view beneath the plaque. However, the use of multi-angle plane wave compounding may be able to enhance the signal underneath some heavily calcified plaques. Ultrasound is also advantageous for the imaging of lipid-rich plaques that may not show up clearly on CTA scans, which is clinically relevant because of the vulnerable nature of plaques high in lipid content.

Finally, a limitation of this study is the fact that two different ultrasound imaging paradigms (focused and plane wave imaging) were used to image the study population. This may have increased the variability of compliance values in particular, given that the lower frame rate and line density achieved with the clinical scanner have been reported to be suboptimal for regional and piecewise PWV estimation (Apostolakis et al. 2017a;

Huang et al. 2014). Furthermore, the lower frame rate may not have been adequate to fully capture the complex waveform of the pulse wave, thus inducing some noise in the detection of the 50% upstroke markers. Plane wave compounding acquisitions are expected to address this issue and aid in the clearer identification of the tracking features. Thus, ongoing PWI studies relying only on high-frame-rate plane wave imaging may be able to differentiate healthy carotid walls from less stenotic lesions such as the moderately calcified plaques presented in this study.

CONCLUSIONS

The results from this pilot clinical study indicate the potential of PWI to differentiate between plaques of varying stiffness, location and composition based on the cumulative displacements, cumulative strains, PWV and compliance. Characteristics such as pulse wave convergence, decreased strain and alternating positive and negative PWVs within the plaque were observed and may serve as valuable information to compensate for the limitations of methods currently used for the assessment of stroke risk.

REFERENCES

Apostolakis IZ, Nandlall SD, Konofagou EE. Piecewise pulse wave imaging (PPWI) for detection and monitoring of focal vascular disease in murine aortas and carotids in vivo. IEEE Trans Med Imaging 2016;35:13–28.
Apostolakis IZ, McGarry MDJ, Bunting EA, Konofagou EE. Pulse wave imaging using coherent compounding in a phantom and in vivo. Phys Med Biol 2017;62:1700–1730.
Apostolakis IZ, Nauleau P, Papadacci C, McGarry MD, Konofagou EE. Feasibility and validation of 4-D pulse wave imaging in phantoms and in vivo. IEEE Trans Ultrason Ferroelectr Freq Control 2017;64:1305–1317.
Bentzon JF, Otsuka F, Virmani R, Falk E. Mechanisms of plaque formation and rupture. Circ Res 2014;114:1852–1866.
Binns RL, Ku DN. Effect of stenosis on wall motion: A possible mechanism of stroke and transient ischemic attack. Arteriosclerosis 1989;9:842–847.
Bleasdale RA, Parker KH, Jones CJH. Chasing the wave: Unfashionable but important new concepts in arterial wave travel. Am J Physiol Circ Physiol 2003;284:H1879–H1885.
Brewin MP, Srodon PD, Greenwald SE, Birch MJ. Carotid atherosclerotic plaque characterisation by measurement of ultrasound sound speed in vitro at high frequency, 20 MHz. Ultrasonics 2014;54:428–441.
Bunting EA, Provost J, Konofagou EE. Stochastic precision analysis of 2-D cardiac strain estimation in vivo. Phys Med Biol 2014;59:6841–6858.
Chan JMS, Monaco C, Wylezinska-Arridge M, Tremoleda JL, Gibbs RGJ. Imaging of the vulnerable carotid plaque: Biological targeting of inflammation in atherosclerosis using iron oxide particles and MRI. Eur J Vasc Endovasc Surg 2014;47:462–469.
Cunha RS, Benetos A, Laurent S, Safar ME, Asmar RG. Distension capacity of the carotid artery and ambulatory blood pressure monitoring: Effects of age and hypertension. Am J Hypertens 1995;8:343–352.
Finn AV, Nakano M, Narula J, Kolodgie FD, Virmani R. Concept of vulnerable/unstable plaque. Arterioscler Thromb Vasc Biol 2010;30:1282–1292.
Fioranelli M, Frajese G. Sports cardiology: From diagnosis to clinical management. Milan/New York: Springer-Verlag Italia; 2012.
Fujikura K, Luo J, Gamarnik V, Pernot M, Fukumoto R, Tilson MD, Konofagou EE. A novel noninvasive technique for pulse-wave imaging and characterization of clinically-significant vascular mechanical properties in vivo. Ultrason Imaging 2007;29:137–154.
Fung YC. Biomechanics: Circulation. 2nd edition New York: Springer-Verlag; 1997.
Gonçalves I, Lindholm MW, Pedro LM, Dias N, Fernandes e Fernandes J, Fredrikson GN, Nilsson J, Moses J, Ares MPS. Elastin and calcium rather than collagen or lipid content are associated with echogenicity of human carotid plaques. Stroke 2004;35:2795–2800.
Grotberg JB, Jensen OE. Biofluid mechanics in flexible tubes. Annu Rev Fluid Mech 2004;36:121–147.
Hansen HHG, de Borst GJ, Bots ML, Moll FL, Pasterkamp G, de Korte CL. Validation of noninvasive in vivo compound ultrasound strain imaging using histologic plaque vulnerability features. Stroke 2016;47 2770−25.
Holzapfel GA. Determination of material models for arterial walls from uniaxial extension tests and histological structure. J Theor Biol 2006;238:290–302.
Huang C, Ren TL, Luo J. Effects of parameters on the accuracy and precision of ultrasound-based local pulse wave velocity measurement: A simulation study. IEEE Trans Ultrason Ferroelectr Freq Control 2014;61:2001–2018.
Hutchinson KJ, Karpinsky E. In vivo demonstration of flow recirculation and turbulence downstream of graded stenoses in canine arteries. J Biomech 1985;18:285–296.
Imparato AM. The carotid bifurcation plaque—A model for the study of atherosclerosis. J Vasc Surg 1986;3:249–255.
Ino-Oka E, Sekino H, Kajikawa S, Satoh T, Inooka H. Evaluation of carotid atherosclerosis from the perspective of blood flow reflection. Clin Exp Hypertens 2009;31:188–200.
Kallel F, Ophir J. A least-squares strain estimator for elastography. Ultrason Imaging 1997;19:195–208.
Khamdaeng T, Luo J, Vappou J, Terdtoon P, Konofagou EE. Arterial stiffness identification of the human carotid artery using the stress−strain relationship in vivo. Ultrasonics 2012;52:402–411.
Konofagou EE, D'hooge J, Ophir J. Myocardial elastography—A feasibility study in vivo. Ultrasound Med Biol 2002;28:475–482.
Korteweg DJ. Ueber die Fortpflanzungsgeschwindigkeit des Schalles in elastischen Röhren. Ann Phys Chem 1878;241:525–542.
Lee WN, Ingrassia CM, Fung-Kee-Fung SD, Costa KD, Holmes JW, Konofagou EE. Theoretical quality assessment of myocardial elastography with in vivo validation. IEEE Trans Ultrason Ferroelectr Freq Control 2007;54:2233–2245.
Lee WN, Konofagou EE. Angle-independent and multi-dimensional myocardial elastography—From theory to clinical validation. Ultrasonics 2008;48:563–567.
Lee SE, Lee SW, Fischer PF, Bassiouny HS, Loth F. Direct numerical simulation of transitional flow in a stenosed carotid bifurcation. J Biomech 2008;41:2551–2561.
Li RX, Luo J, Balaram SK, Chaudhry FA, Shahmirzadi D, Konofagou EE. Pulse wave imaging in normal, hypertensive and aneurysmal human aortas in vivo: A feasibility study. Phys Med Biol 2013;58:4549–4562.
Li RX, Qaqish W, Konofagou EE. Performance assessment of pulse wave imaging using conventional ultrasound in canine aortas ex vivo and normal human arteries in vivo. Artery Res 2015;11:19–28.
Libby P, Ridker PM, Hansson GK. Progress and challenges in translating the biology of atherosclerosis. Nature 2011;473:317–325.
Lovett JK, Gallagher PJ, Hands LJ, Walton J, Rothwell PM. Histological correlates of carotid plaque surface morphology on lumen contrast imaging. Circulation 2004;110:2190–2197.
Lovett JK, Gallagher PJ, Rothwell PM. Reproducibility of histological assessment of carotid plaque: Implications for studies of carotid imaging. Cerebrovasc Dis 2004;18:117–123.

Luo J, Fujikura K, Tyrie LS, Tilson MD, Konofagou EE. Pulse wave imaging of normal and aneurysmal abdominal aortas in vivo. IEEE Trans Med Imaging 2009;28:477–486.

Luo J, Konofagou E. A fast normalized cross-correlation calculation method for motion estimation. IEEE Trans Ultrason Ferroelectr Freq Control 2010;57:1347–1357.

Luo J, Konofagou EE. Imaging of wall motion coupled with blood flow velocity in the heart and vessels in vivo: A feasibility study. Ultrasound Med Biol 2011;37:980–995.

Luo J, Li RX, Konofagou EE. Pulse wave imaging of the human carotid artery: an in vivo feasibility study. IEEE Trans Ultrason Ferroelectr Freq Control 2012;59:174–181.

Mahmoud AM, Dutta D, Lavery L, Stephens D, Villanueva FS, Kim K. Noninvasive detection of lipids in atherosclerotic plaque using ultrasound thermal strain imaging: In vivo animal study. J Am Coll Cardiol 2013;62:1804–1809.

McGarry M, Li R, Apostolakis I, Nauleau P, Konofagou EE. An inverse approach to determining spatially varying arterial compliance using ultrasound imaging. Phys Med Biol 2016;61: 5486–5507.

McGarry M, Nauleau P, Apostolakis I, Konofagou E. In vivo repeatability of the pulse wave inverse problem in human carotid arteries. J Biomech 2017;64:136–144.

Meinders J, Brands P, Willigers J, Kornet L, Hoeks AP. Assessment of the spatial homogeneity of artery dimension parameters with high frame rate 2-D B-mode. Ultrasound Med Biol 2001;27:785–794.

Moens A. Die Pulscurve. Available at: https://archive.org/details/die-pulscurve00iseb; 1878 Accessed November 10, 2017.

Moller MJ, Qin Z, Toursarkissian B. Tissue markers in human atherosclerotic carotid artery plaque. Ann Vasc Surg 2012;26:1160–1165.

Mughal MM, Khan MK, DeMarco JK, Majid A, Shamoun F, Abela GS. Symptomatic and asymptomatic carotid artery plaque. Expert Rev Cardiovasc Ther 2011;9:1315–1330.

Naghavi M, Libby P, Falk E, Casscells SW, Litovsky S, Rumberger J, Badimon JJ, Stefanadis C, Moreno P, Pasterkamp G, Fayad Z, Stone PH, Waxman S, Raggi P, Madjid M, Zarrabi A, Burke A, Yuan C, Fitzgerald PJ, Siscovick DS, de Korte CL, Aikawa M, Juhani Airaksinen KE, Assmann G, Becker CR, Chesebro JH, Farb A, Galis ZS, Jackson C, Jang I-K, Koenig W, Lodder RA, March K, Demirovic J, Navab M, Priori SG, Rekhter MD, Bahr R, Grundy SM, Mehran R, Colombo A, Boerwinkle E, Ballantyne C, Insull W, Schwartz RS, Vogel R, Serruys PW, Hansson GK, Faxon DP, Kaul S, Drexler H, Greenland P, Muller JE, Virmani R, Ridker PM, Zipes DP, Shah PK, Willerson JT. From vulnerable plaque to vulnerable patient: A call for new definitions and risk assessment strategies, Part I. Circulation 2003;108:1664–1672.

Naim C, Cloutier G, Mercure E, Destrempes F, Qin Z, El-Abyad W, Lanthier S, Giroux MF, Soulez G. Characterisation of carotid plaques with ultrasound elastography: Feasibility and correlation with high-resolution magnetic resonance imaging. Eur Radiol 2013;23:2030–2041.

Nandlall SD, Konofagou EE. Assessing the stability of aortic aneurysms with pulse wave imaging. Radiology 2016;281:772–781.

Nichols WW, Denardo SJ, Wilkinson IB, McEniery CM, Cockcroft J, O'Rourke MF. Effects of arterial stiffness, pulse wave velocity, and wave reflections on the central aortic pressure waveform. J Clin Hypertens (Greenwich) 2008;10:295–303.

Nichols WW, O'Rourke MF, Vlachopoulos C. McDonald's blood flow in arteries: Theoretical, experimental and clinical principles. 6th edition Boca Raton, FL: CRC Press; 2011.

Oliver TB, Lammie GA, Wright AR, Wardlaw J, Patel SG, Peek R, Ruckley CV, Collie DA. Atherosclerotic plaque at the carotid bifurcation: CT angiographic appearance with histopathologic correlation. AJNR Am J Neuroradiol 1999;20:897–901.

Ophir J, Alam SK, Garra B, Kallel F, Konofagou E, Krouskop T, Varghese T. Elastography: Ultrasonic estimation and imaging of the elastic properties of tissues. Proc Inst Mech Eng Part H J Eng Med 1999;213:203–233.

Park S, Lee SW, Lim OK, Min I, Nguyen M, Ko YB, Yoon K, Suh DC. Computational modeling with fluid−structure interaction of the

severe M1 stenosis before and after stenting. Neurointervention 2013;8:23–28.

Perktold K, Rappitsch G. Computer simulation of local blood flow and vessel mechanics in a compliant carotid artery bifurcation model. J Biomech 1995;28:845–856.

Polak JF, Johnson C, Harrington A, Wong Q, O'Leary DH, Burke G, Yanez ND. Changes in carotid intima−media thickness during the cardiac cycle: The multi-ethnic study of atherosclerosis. J Am Heart Assoc 2012;1 e001420.

Poree J, Garcia D, Chayer B, Ohayon J, Cloutier G. Noninvasive vascular elastography with plane strain incompressibility assumption using ultrafast coherent compound plane pave imaging. IEEE Trans Med Imaging 2015;34:2618–2631.

Provost J, Lee WN, Fujikura K, Konofagou EE. Imaging the electromechanical activity of the heart in vivo. Proc Natl Acad Sci USA 2011;108:8565–8570.

Ross R. The pathogenesis of atherosclerosis: A perspective for the 1990s. Nature 1993;362:801–809.

Roy Cardinal MH, Heusinkveld MHG, Qin Z, Lopata RGP, Naim C, Soulez G, Cloutier G. Carotid artery plaque vulnerability assessment using noninvasive ultrasound elastography: Validation with MRI. Am J Roentgenol 2017;209:142–151.

Saba L, Anzidei M, Marincola BC, Piga M, Raz E, Bassareo PP, Napoli A, Mannelli L, Catalano C, Wintermark M. Imaging of the carotid artery vulnerable plaque. Cardiovasc Intervent Radiol 2014;37: 572–585.

Schulz UG, Rothwell PM. Major variation in carotid bifurcation anatomy: A possible risk factor for plaque development. Stroke 2001;32:2522–2529.

Segers P, Rabben SI, De Backer J, De Sutter J, Gillebert TC, Van Bortel L, Verdonck P. Functional analysis of the common carotid artery: Relative distension differences over the vessel wall measured in vivo. J Hypertens 2004;22:973–981.

Shahmirzadi D, Konofagou EE. Pulse-Wave Propagation in Straight-Geometry Vessels for Stiffness Estimation: Theory, Simulations, Phantoms and In Vitro Findings. J. Biomech Eng. 2012;134(11): 114502.

Strandness DE. Atherosclerotic plaques: Advances in imaging for sequential quantitative evaluation. J Vasc Surg 1994;19:368.

Tan FPP, Soloperto G, Bashford S, Wood NB, Thom S, Hughes A, Xu XY. Analysis of flow disturbance in a stenosed carotid artery bifurcation using two-equation transitional and turbulence models. J Biomech Eng 2008;130:61008.

Tang D, Yang C, Kobayashi S, Zheng J, Vito RP. Effect of stenosis asymmetry on blood flow and artery compression: A three-dimensional fluid−structure interaction model. Ann Biomed Eng 2003;31:1182–1193.

Taussky P, Hanel RA, Meyer FB. Clinical considerations in the management of asymptomatic carotid artery stenosis. Neurosurg Focus 2011;31:E7.

Teng Z, Canton G, Yuan C, Ferguson M, Yang C, Huang X, Zheng J, Woodard PK, Tang D. 3-D critical plaque wall stress is a better predictor of carotid plaque rupture sites than flow shear stress: An in vivo MRI-based 3-D FSI study. J Biomech Eng 2010;132:31007.

Underhill HR, Hatsukami TS, Cai J, Yu W, DeMarco JK, Polissar NL, Ota H, Zhao X, Dong L, Oikawa M, Yuan C. A noninvasive imaging approach to assess plaque severity: the carotid atherosclerosis score. AJNR Am J Neuroradiol 2010;31:1068–1075.

van den Oord SCH, Akkus Z, Renaud G, Bosch JG, van der Steen AFW, Sijbrands EJG, Schinkel AFL. Assessment of carotid atherosclerosis, intraplaque neovascularization, and plaque ulceration using quantitative contrast-enhanced ultrasound in asymptomatic patients with diabetes mellitus. Eur Heart J Cardiovasc Imaging 2014;15: 1213–1218.

Vappou J, Luo J, Konofagou EE. Pulse wave imaging for noninvasive and quantitative measurement of arterial stiffness in vivo. Am J Hypertens 2010;23:393–398.

Wasserman BA, Wityk RJ, Trout HH, Virmani R. Low-grade carotid stenosis: Looking beyond the lumen with MRI. Stroke 2005;36:2504–2513.

Watanabe H, Yamazaki N, Kobayashi Y, Miyashita T, Ohdaira T, Hashizume M, Fujie MG. Estimation of intraoperative blood flow during liver RF ablation using a finite element method-based biomechanical simulation. In: Proceedings, 2011 Annual International Conference of the IEEE Engineering in Medicine and Biology Society. New York. : IEEE; 2011. p. 7441–7445.

Westenberg JJM, van Poelgeest EP, Steendijk P, Grotenhuis HB, Jukema JW, de Roos A. Bramwell−Hill modeling for local aortic pulse wave velocity estimation: A validation study with velocity-encoded cardiovascular magnetic resonance and invasive pressure assessment. J Cardiovasc Magn Reson 2012;14:2.

Xu D, Hippe DS, Underhill HR, Oikawa-Wakayama M, Dong L, Yamada K, Yuan C, Hatsukami TS. Prediction of high-risk plaque development and plaque progression with the carotid atherosclerosis score. JACC Cardiovasc Imaging 2014;7:366–373.

Zaleska-Dorobisz U, Kaczorowski K, Pawluś A, Puchalska A, Inglot M. Ultrasound elastography: Review of techniques and its clinical applications. Adv Clin Exp Med 2014;23:645–655.

Zhang S, Levin DC, Halpern EJ, Fischman D, Savage M, Walinsky P. Accuracy of MDCT in assessing the degree of stenosis caused by calcified coronary artery plaques. Am J Roentgenol 2008;191:1676–1683.